# Catalytic Membrane Reactor for Suzuki-Miyaura C−C Cross-Coupling: Explanation for Its High Efficiency via Modeling

**Yingying Gu, Patrice Bacchin, Jean-François Lahitte, and Jean-Christophe Remigy**
Laboratoire de Génie Chimique, INPT, UPS, UMR CNRS 5503, Université de Toulouse, 118
Route de Narbonne F-31062 Toulouse, France

**Isabelle Favier and Montserrat Gómez**
Laboratoire Hétérochimie Fondamentale et Appliquée, UMR CNRS 5069, Université de Toulouse
3 – Paul Sabatier, 118 route de Narbonne, F-31062 Toulouse, France

**Douglas L. Gin and Richard D. Noble**
Dept. of Chemical & Biological Engineering, University of Colorado, Boulder, CO 80309, and Dept. of Chemistry & Biochemistry, University of Colorado, Boulder, CO 80309

*A polymeric catalytic membrane was previously prepared that showed remarkable efficiency for Suzuki-Miyaura C-C cross-coupling in a flow-through configuration. A mathematic model was developed and fitted to the experimental data to understand the significant apparent reaction rate increase exhibited by the catalytic membrane reactor compared to the catalytic system under batch reaction conditions. It appears that the high palladium nanoparticles concentration inside the membrane is mainly responsible for the high apparent reaction rate achieved. In addition, the best performance of the catalytic membrane could be achieved only in the forced flow-through configuration, that, conditions permitting to the reactants be brought to the catalytic membrane by convection.* © 2016 American Institute of Chemical Engineers *AIChE J*, 63: 698–704, 2017
*Keywords: polymeric catalytic membrane, palladium nanoparticles, forced flow-through, modeling, mechanism*

## Introduction

Catalytic membranes have been extensively studied in the last two decades because they represent a process intensification. More recently, catalytic polymeric membranes, which were less studied than inorganic ones, have attracted growing interest because of their relatively low cost and high efficiency.[1] They were found catalytically active on a variety of reactions (e.g., alcohol and ether syntheses,[2] C-C cross-couplings[3–5] hydrogenations,[6] chemical reductions[7,8]). Some polymeric catalytic membranes even gave full conversion of substrates within residence time of seconds,[3,8] showing prospective potential of the catalytic polymeric membranes containing palladium nanoparticles (PdNPs). Whereas there is a lack of investigations into the reasons why those polymeric catalytic membranes are so efficient. This understanding is undoubtedly important to provide guidelines to design catalytic membrane reactors.

One major type of catalytic membrane reactors are membrane contactors. Due to their nonpermselectivity toward reactants and products, membrane contactors can offer higher throughput than extractor and distributor catalytic membranes. It is generally accepted that main function of membrane contactors consists of favoring mass transfer by intensifying the contact between reactants and catalyst.[9,10] Nagy established several mathematical models to study the mass transfer accompanied by reactions in the catalytic membrane.[11] Herein, we deduced using a similar model that the intensified contact between catalyst and reactants was not the only factor responsible for the high catalytic activity observed in a forced-flow membrane contactor using a catalytic membrane with immobilized PdNPs. The results obtained provide further understanding into the principles involved in catalytic membrane contactors. In this work, PdNPs were used as catalyst for their catalytic performance, especially in carbon–carbon bond formation.[12]

## Materials and Methods

### *Catalytic polymeric membrane, PdNPs colloidal solution and the corresponding Pd-catalyzed Suzuki-Miyaura C-C cross-coupling reactions were previously reported[3]*

The catalytic membrane was prepared through the functionalization of a microfiltration membrane whose nominal pore size is 0.2 $\mu$m, with a very narrow pore-size distribution.

To run the reaction using the catalytic membrane, the reaction mixture was premixed and then filtered through the membrane. The permeate flow rate was varied by using the peristaltic pump (with the flux density $j$ fell in the range of $27$–$1300\,\text{L}\,\text{h}^{-1}\,\text{m}^{-2}$). The transmembrane pressure was in the range of $1$–$150$ mbar. The mean flow velocity inside the membrane $v_m$ can be calculated as $v_m = j/\varepsilon$, with $\varepsilon$ as membrane porosity, which is considered to be 0.8 in our case. As for the calculation of the flow velocity in the bulk solution, porosity is taken as 1.

The same reaction was carried out under batch conditions using a PdNPs colloidal solution.

### Mass-transfer model for the catalytic membrane

The fluid followed a laminar flow pattern in the membrane pores (pore size $\leq 0.2\,\mu\text{m}$), giving rise to a parabolic velocity profile. When the radial diffusion across the pore is much faster than convective mass transfer in the axial direction, the parabolic flow velocity profile can be reconciled with plug flow behavior (flat concentration profile).[13–15] For our catalytic membrane, the residence time was $10^4$ to $10^5$ longer than the characteristic mixing time (to diffuse halfway across the pore, $\tau_{\text{mix}} = \frac{d^2}{4D}$, with $d$ as pore diameter $0.2\,\mu\text{m}$ and $D$ as diffusion coefficient). Hence, a plug flow pattern was readily achieved inside the membrane, permitting a simplification of modeling of the catalytic membrane to one dimension (the concentration can be considered as homogeneous in a slice of the membrane parallel to the surface). The external mass-transfer resistance through the boundary layer around the catalyst was neglected (concentration on the catalyst surface equals to the bulk concentration, see section the Calculations on Mass-Transfer Resistance). Since the PdNPs are dense particles (unlike porous pellets), no internal diffusion needs to be considered. In addition, isothermal conditions (fluid and membrane temperature were constant and in complete agreement) were also achieved under the experimental conditions according to Westernmann's model.[16] Therefore, a constant intrinsic reaction rate $k_{\text{mem}}$ was imposed. The differential mass balance for the catalytic membrane at steady state taking into consideration the convective flow, diffusion and a first-order reaction can be then expressed by Eq. 1.

$$D\frac{d^2C}{dz^2} - v_{\text{m}}\frac{dC}{dz} - ak_{\text{mem}}C = 0 \tag{1}$$

where $D$ is the diffusion coefficient ($4.1 \times 10^{-10}\,\text{m}^2\,\text{s}^{-1}$); $v_{\text{m}}$ is the convective velocity inside the membrane; $C$ is concentration of the limiting reactant (1-iodo-4-nitrobenzene); $a$ is the specific surface area of the catalyst (total catalyst surface area divided by the membrane volume, $\text{m}^2\,\text{m}^{-3}$); $k_{\text{mem}}$ is the surface intrinsic reaction rate constant; and $z$ is the space coordinate. The $D$ value of the solute molecules at $60°\text{C}$ can be calculated by the Stokes-Einstein equation (Eq. 2)

$$D = \frac{k_{\text{B}}T}{6\pi\mu r} \tag{2}$$

where $k_{\text{B}}$ is Boltzmann's constant; $T$ is the absolute temperature; $\mu$ is the dynamic viscosity of the solvent ($5.9 \times 10^{-4}\,\text{kg}\,\text{m}^{-1}\,\text{s}^{-1}$ for ethanol at $60°\text{C}$[17]); and $r$ is the solute molecule radius (on the order of 1 nm).

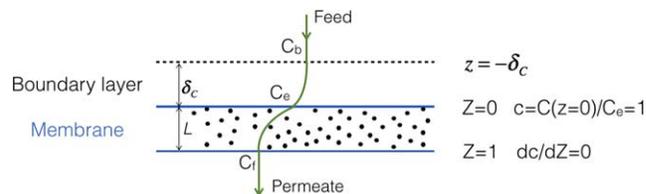Equation 1 can be transformed into Eq. 3:



**Figure 1. Schematic representation of the modeled catalytic membrane (black dots representing PdNPs; figure components not drawn to scale).**

[Color figure can be viewed in the online issue, which is available at wileyonlinelibrary.com.]

$$\frac{d^2c}{dZ^2} - Pe_{\text{M}} \cdot \frac{dc}{dZ} - \varnothing^2 c = 0 \tag{3}$$

where $c\ (=C/C_{\text{e}})$ and $Z\ (=z/L)$ are the dimensionless concentration and coordinates, respectively, with $C_{\text{e}}$ being the limiting reactant concentration on the feed side surface of the membrane and $L$ being the membrane thickness. $Pe_{\text{M}}$ is the Péclet number for mass transfer inside the membrane ($Pe_{\text{M}} = v_{\text{m}}L/D$); and $\varnothing$ is the Thiele modulus $\varnothing = \sqrt{\frac{ak_{\text{mem}}}{D}}L$.[18] The boundary conditions for this differential equation are[18] (Figure 1):

$$Z = 0 : \quad c = 1 \tag{4}$$

$$Z = 1 : \quad \frac{dc}{dZ} = 0 \tag{5}$$

The solution for Eq. 3 is therefore:

$$c = \frac{e^{\frac{Pe_{\text{M}} - \sqrt{\Delta}}{2}Z}}{1 - \frac{Pe_{\text{M}} - \sqrt{\Delta}}{Pe_{\text{M}} + \sqrt{\Delta}}e^{-\sqrt{\Delta}}} + \frac{e^{\frac{Pe_{\text{M}} + \sqrt{\Delta}}{2}Z}}{1 - \frac{Pe_{\text{M}} + \sqrt{\Delta}}{Pe_{\text{M}} - \sqrt{\Delta}}e^{\sqrt{\Delta}}} \tag{6}$$

where

$$\Delta = Pe_{\text{M}}^2 + 4\varnothing^2 \tag{7}$$

When there exists a concentration boundary layer of a thickness $\delta_C$ over the feed side of the membrane, a concentration gradient in the boundary layer is produced, and $C_{\text{e}}$ does not equal to the limiting reactant concentration in the bulk solution $C_{\text{b}}$ (Figure 1). The conversion $X$ can be then expressed as:

$$X = 1 - \frac{C_{\text{f}}}{C_{\text{b}}} = 1 - \frac{C_{\text{e}}}{C_{\text{b}}} \cdot \frac{C_{\text{f}}}{C_{\text{e}}} = 1 - \frac{C_{\text{e}}}{C_{\text{b}}} \cdot c|_{Z=1} \tag{8}$$

where $C_{\text{f}}$ is the limiting reactant concentration at $Z = 1$.

The differential mass balance in the concentration boundary layer without reaction at steady state can be given by:

$$D\frac{d^2C}{dz^2} - v\frac{dC}{dz} = 0 \tag{9}$$

with boundary conditions:

$$C\big|_{z=-\delta_C} = C_{\text{b}} \tag{10}$$

$$C\big|_{z=0} = C_{\text{e}} \tag{11}$$

and $v$ as the convective velocity in the bulk solution.

The mass-transfer flux $J$ can be obtained by means of Eq. 12, taking into account both the diffusive and the convective flows as follows:

$$J = -D\frac{dC}{dz} + vC \tag{12}$$

The relation between $C_e$ and $C_b$ can be thus deduced from Eqs. 9 to 12 as:

$$C_e = \frac{J|_{z=0}}{v} \cdot (1 - e^{Pe_{BL}}) + C_b \cdot e^{Pe_{BL}} \tag{13}$$

where $Pe_{BL}$ is the Péclet number of the concentration boundary layer: $Pe_{BL} = v\delta_C/D$. The concentration boundary layer thickness is a function of the momentum boundary layer thickness $\delta$ and Schmidt number[19,20] (Eqs. 14 and 15):[20]

$$\delta = \sqrt{\frac{\mu}{\rho\omega}} = 190 \ \mu m \tag{14}$$

where $\omega$ is the agitation velocity (22 rad s$^{-1}$), and $\mu$ and $\rho$ are the dynamic viscosity and density of the solution, respectively.

$$\delta_C = \delta/Sc^{\frac{1}{3}} = 15.4 \ \mu m \tag{15}$$

We denote $Sh$ as $Sh = J|_{z=0} \cdot Pe_M/(v_m \cdot C_e)$. Then from Eqs. 6 to 12, the expression of $Sh$ can be deduced as:

$$Sh = \varepsilon Pe_M - \frac{\frac{Pe_M - \sqrt{\Delta}}{2}}{1 - \frac{Pe_M - \sqrt{\Delta}}{Pe_M + \sqrt{\Delta}} e^{-\sqrt{\Delta}}} - \frac{\frac{Pe_M + \sqrt{\Delta}}{2}}{1 - \frac{Pe_M + \sqrt{\Delta}}{Pe_M - \sqrt{\Delta}} e^{\sqrt{\Delta}}} \tag{16}$$

By combining Eq. 13 with Eq. 16, the ratio of $C_e/C_b$ can be given as follows:

$$\frac{C_e}{C_b} = \frac{e^{Pe_{BL}}}{1 - \frac{Sh}{Pe_M} \cdot \frac{1}{\varepsilon}(1 - e^{Pe_{BL}})}$$

$$= \frac{e^{Pe_{BL}}}{1 - \left(1 - \frac{Pe_M - \sqrt{\Delta}}{2\varepsilon \cdot A \cdot Pe_M} - \frac{Pe_M + \sqrt{\Delta}}{2\varepsilon \cdot B \cdot Pe_M}\right) \cdot (1 - e^{Pe_{BL}})} \tag{17}$$

where

$$A = 1 - \frac{Pe_M - \sqrt{\Delta}}{Pe_M + \sqrt{\Delta}} \cdot e^{-\sqrt{\Delta}} \tag{18}$$

$$B = 1 - \frac{Pe_M + \sqrt{\Delta}}{Pe_M - \sqrt{\Delta}} \cdot e^{\sqrt{\Delta}} \tag{19}$$

The concentration profile inside the concentration boundary layer can be obtained based on Eqs. 9–11 as follows:

$$C_{BL} = \frac{e^{Pe_{BL} \cdot Y/2}}{\sinh(Pe_{BL}/2)}$$
$$\left[\sinh\left(Pe_{BL} \cdot \frac{1-Y}{2}\right) \cdot C_b + e^{-Pe_{BL}/2} \cdot \sinh\left(Pe_{BL} \cdot \frac{Y}{2}\right) \cdot C_e\right] \tag{20}$$

with $Y = (z+\delta)/\delta$.

## Results and Discussion
### Reaction regime of the colloidal solution

The Stokes number of the colloidal system was calculated to be $5 \times 10^{-12}$, indicating that the PdNPs follow the streamline so closely that the relative velocity between PdNPs and the liquid phase is nearly zero.[3] Thus, the convection becomes inefficient and actually negligible. The mass transfer is therefore effectuated only by diffusion. The mass-transport coefficient ($k_d^b$ in the batch reactor) and the diffusion coefficient ($D$) can be correlated by the Sherwood number $Sh$ (Eq. 21), which can be calculated using Eq. 22.[21,22]

$$\frac{k_d^b \cdot d_p}{D} = Sh \tag{21}$$

$$Sh = 2 + \frac{d_p}{\sqrt{\pi Dt}} \approx 2 \tag{22}$$

where $d_p$ is the diameter of PdNPs. At $t > 1 \times 10^{-3}$ s, then $d_p/\sqrt{\pi Dt} < 0.02$, and hence $Sh \cong 2$. $D = 1.22 \times 10^{-11}$ m$^2$ s$^{-1}$ for the colloidal system ($\mu \approx 2.0 \times 10^{-2}$ kg m$^{-1}$ s$^{-1}$ for the IL at 60°C[23,24].

The mass-transfer coefficient was calculated to be:

$$k_d^b = 5.8 \times 10^{-3} \ m \ s^{-1} \tag{23}$$

The boundary layer thickness around the particle is hence $\delta_p = D/k_d^b = 2$ nm. The specific surface area $a$ (total surface area of the PdNPs divided by the reaction mixture volume, m$^2$ m$^{-3}$) of the colloidal system was estimated to be in the range of $5.3 \times 10^3$ m$^2$ m$^{-3}$ to $3.6 \times 10^5$ m$^2$ m$^{-3}$ (i.e., the PdNP mean diameter varying from 4 nm to 100 nm, taking into consideration the presence of aggregates). The mass-transfer flux ($a \cdot k_d^b$, s$^{-1}$) was thus found much higher (five to seven orders of magnitude greater) than the apparent reaction-rate constant. Therefore, the activity of the colloidal system was in reaction-limited regime. The intrinsic kinetic $a \cdot k_{batch}$ value was approximately the same as the apparent kinetics (Eq. 24).

$$a \cdot k_{batch} \approx k_{app} = 2.3 \times 10^{-4} \ s^{-1} \tag{24}$$

The intrinsic reaction-rate constant on the catalyst surface for the batch reactor $k_{batch}$ was estimated to be in the range of $6.0 \times 10^{-10}$ m s$^{-1}$ to $4.1 \times 10^{-8}$ m s$^{-1}$. (The exact value of specific surface area $a$ cannot be determined; only a range could be given, see above.). This means that the concentration on the PdNP surface could be considered to be the same as the bulk concentration ($k_{batch}/k_d^b \ll 1$).

### Proposed mechanism of operation of the catalytic membrane

*Calculations on Mass-Transfer Resistance.* The mass-transfer coefficient around the catalyst supported on the membrane $k_d^m$ can be estimated by Eq. 25 and found to be 0.41 m s$^{-1}$, which is much larger than that in batch reactor $k_d^b$ ($5.8 \times 10^{-3}$ m s$^{-1}$). Calculations deduced from $Sh = 2$ (which is also valid for the catalytic membrane[25] gives the same $k_d^m$ value. The intrinsic reaction rate constant should be approximately the same for PdNPs in the batch reactor and inside the membrane (maybe lightly higher in the membrane since NPs in the membranes are smaller). The mass-transfer resistance imposed by the boundary layer around the catalyst particles is therefore also negligible in the case of the catalytic membrane.

$$k_d^m = D/e = 0.41 \ m \ s^{-1} \tag{25}$$

In Eq. 25, $D$ is the limiting reactant diffusion coefficient in ethanol at 60°C, $4.1 \times 10^{-10}$ m$^2$ s$^{-1}$, since obvious swelling of the poly(IL) occurs in ethanol (i.e., the diffusion coefficient is mainly determined by the solvent viscosity when the molecule size is smaller than polymer correlation length $\xi$[26]; and $e$ the boundary layer thickness, considered to be half interparticle distance ($e \approx 1$ nm). Even if $D$ is 100 times smaller, the mass-transfer resistance imposed by the boundary layer around the catalyst would still not be a limiting factor.

*Reaction Kinetics.* The Suzuki-Miyaura cross-coupling reaction was tested at different flow rates at 60°C with a 1-iodo-4-nitrobenzene concentration of 0.016 mol L$^{-1}$.
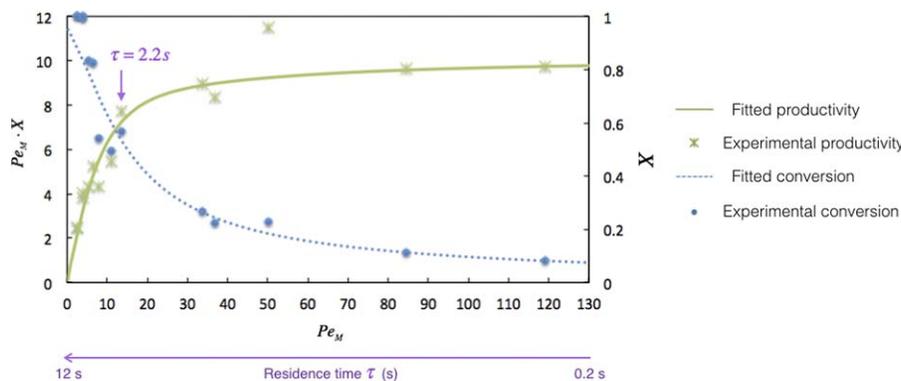
**Figure 2. Concentration profiles along the coordinate at various flow rates (simulated by the model).**

X = conversion (based on 1-iodo-4-nitrobenzene consumption).

Conversion and productivity (interpreted as the product of Péclet number inside the membrane and conversion) were plotted as a function of Péclet number inside the membrane (Figure 2). When flow rate increased (reflected by the increase of the Péclet number inside the membrane), the conversion decreased while the productivity increased.

According to the model described in the Materials and Methods section (Eqs. 6–8, 17), the conversion is a function of Péclet numbers, Thiele modulus and membrane porosity: $X=f(Pe_M, \varnothing, Pe_{BL}, \varepsilon)$. Hence, Thiele modulus is the only unknown parameter. By fitting the model to the experimental data, Thiele modulus, $\varnothing=\sqrt{\frac{ak_{mem}}{D}}L$, was deduced to be 3.19. This result indicates that the reaction is still limited by diffusion along the membrane thickness. By taking the diffusion coefficient of ethanol at 60°C, the apparent reaction rate constant was deduced to be:

$$k_{app}=ak_{mem}=3.4\times10^{-1}s^{-1} \qquad (26)$$

When normalized to the PdNP mass and surface area, the apparent reaction-rate constant is then 431 s$^{-1}$ g$^{-1}$ and 0.53 s$^{-1}$ m$^{-2}$. Compared with catalytic batch reaction conditions (where $k_{app,batch}= 0.22$ s$^{-1}$ g$^{-1}$), the catalytic membrane reactor exhibited an acceleration of the apparent reaction rate by three orders of magnitude.

The specific catalyst surface in the membrane was calculated as $a=4.66\times10^6$ m$^2$ m$^{-3}$; and hence, the intrinsic reaction rate constant on the catalyst supported on the membrane is $k_{mem}=7.4\times10^{-8}$ m s$^{-1}$, which is the same order of magnitude as corresponding value $k_{batch}$ in the batch reactor.

### Concentration profiles

Once the ratio of $C_e$ to $C_b$ is determined from Eq. 17, concentration profiles in the boundary layer and in the membrane can be plotted as a function of flow velocity using Eq. 20 and Eqs. 6-8. Figure 2 shows the concentration profiles in the concentration boundary layer at the feed side and inside the membrane, predicted by the model with $\varnothing=3.19$ at different residence times (flow rates or Péclet numbers). The concentration boundary layer significantly reduced the diffusion flux from the bulk solution to the membrane surface and became a limiting step.

At high flow rates ($Pe_{BL} \geq 1.5$), the convection was largely dominant over diffusion. The reactant was effectively brought to the membrane surface by convection so that $C_e \approx C_b$. Higher flow rates also lead to the increase of reactant

concentration inside the membrane?thus increasing the productivity. However, the short residence time was insufficient to achieve full conversion. For Péclet numbers smaller than 1.5, the reaction was limited by diffusion. The concentration at the membrane feed surface $C_e$ differentiated from the bulk solution concentration $C_b$ ($C_e < C_b$), less reactants reached the inside of the membrane, exerting negative influence on the productivity.

As shown in Figure 3, the reaction productivity increased with the flux until the convection became largely dominant, where a maximum plateau was thus reached. The transition Péclet value ($Pe_{BL}=1.5$) where ($C_b-C_e$) became less noticeable corresponded to the flux (146 L h$^{-1}$ m$^{-2}$) from which the productivity began to approach the maximum plateau. The reaction on the membrane became kinetically limited at maximum productivity.
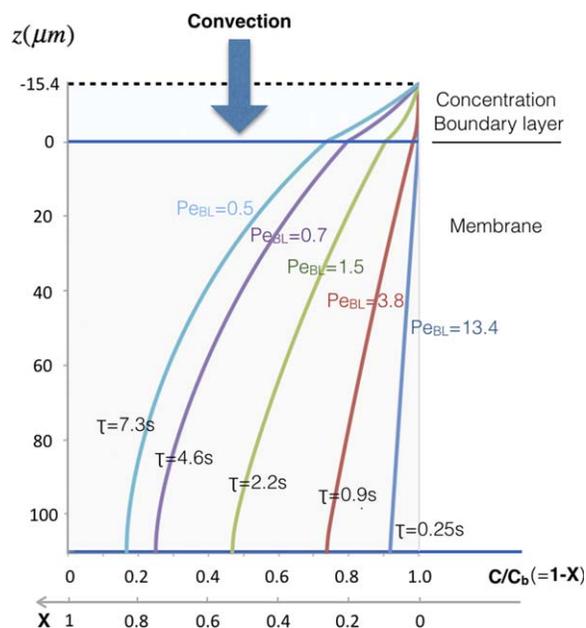


**Figure 3.** Variation in dimensionless productivity ($Pe_M \cdot X$) and conversion ($X$) values as a function of Péclet number for the catalytic membrane reactor at 60°C.

**Table 1. Comparison Between the Batch Reactor and the Catalytic Membrane Reactor: PdNPs Size and Distribution and Performance on Suzuki-Miyaura Cross-Coupling Between 1-Iodo-4-Nitrobenzene and Phenyboronic Acid**

| Entry | | Batch Reactor | Flow-through Membrane Reactor | Comparative Factor[a] |
|---|---|---|---|---|
| 1 | PdNPs size (nm) | $4 \pm 2$ | $2 \pm 1$ | 1/2 |
| 2 | Interparticle distance (nm) | 50–100 | ca. 2 | 1/50–1/25 |
| 3 | Number of PdNP (mm$^{-3}$)[b] | $1.7 \times 10^{8}$ to $2.8 \times 10^{12}$[c] | $1.4 \times 10^{14}$ to $4.0 \times 10^{14}$[d] | $\geq 143$[e] |
| 4 | Estimated total catalyst surface area $S$ (m$^2$) | 0.36 | 0.64 | 1.8 |
| 5 | $S$/substrate ratio (m$^2$ mol$^{-1}$) | 5–364 | $3.6 \times 10^{5}$[f] | >1000 |
| 6 | Reaction time for full conversion[g] | 6 h | <10 s | 1/2160 |
| 7 | Selectivity (%)[h] | 92 | 100 | 1.09 |
| 8 | $k_{app}$ (s$^{-1}$) | $2.3 \times 10^{-4}$ | $3.4 \times 10^{-1}$ | 1528 |
| 9 | $k_{app}/m_{Pd}$ (s$^{-1}$ g$^{-1}$)[i] | 0.22 | 431 | 2038 |
| 10 | $k_{app}/S$ (s$^{-1}$ m$^{-2}$)[f] | $6.2 \times 10^{-4}$ to $4.2 \times 10^{-2}$ | $5.3 \times 10^{-1}$ | 12–864 |
| 11 | $a$ (m$^2$ m$^{-3}$)[j] | $5.3 \times 10^{3}$ to $3.6 \times 10^{5}$ | $4.66 \times 10^{6}$ | 13–879 |
| 12 | $k$ (m s$^{-1}$)[k] | $6.2 \times 10^{-10}$ to $4.2 \times 10^{-8}$ | $7.4 \times 10^{-8}$ | $\geq 1.7$ |

[a](catalytic membrane reactor)/(batch reactor) value ratio.
[b]Number of palladium particles/aggregates per unit volume.
[c]Values calculated taken into consideration the presence of aggregates (diameter = 4–100 nm).
[d]Value for reactive zones where palladium is highly concentrated ($4.0 \times 10^{14}$) and an average value obtained by (amount of Pd)/(membrane volume) ($1.4 \times 10^{14}$).
[e]$143 = 4.2 \times 10^{14}/2.8 \times 10^{12}$ (comparative factor between the reactive zone of the membrane and the Pd concentration in the batch reactor calculated with $d = 4$ nm). The ratio between the reactive zone of the membrane and the batch system taking into consideration the presence of aggregates in the latter should be in the range of $143 - 2.35 \times 10^{6}$.
[f]Local ratio inside the membrane environment, porosity = 0.8.
[g]In the membrane reactor, the reaction time is defined as the contact time of reagents with the membrane.[3]
[h]Selectivity toward the cross-coupling product.
[i]Apparent reaction rate constant normalized to palladium mass.
[j]Specific surface: catalyst surface area divided by the reactor volume.
[k]Intrinsic reaction rate constant on the catalyst surface.

## *Comparative study between the catalytic membrane reactor and PdNP colloidal solution in the batch reactor and proposed explanation for the high efficiency of the catalytic membrane reactor*

The differences between the colloidal system (with PdNPs dispersed in [MMPIM][NTf$_2$], 1,2-dimethyl-3-propylimidazolium bis(trifluoromethylsulfonyl)imide) in batch reactor and the catalytic membrane reactor are summarized in Table 1. The catalytic membrane reactor works with higher efficiency (entry 6) and selectivity (entry 7) than the colloidal system. The apparent reaction constants of the two systems were given in entry 8. The values normalized to catalyst surface were also given (entry 10). The apparent reaction constant is almost 2000 times larger in the catalytic membrane with the same amount of palladium (entry 9). This result can be attributed to the fact that palladium nanoparticles are well-dispersed and distributed very close to each other inside the membrane (with small interparticle distances, entry 2), leading to an extremely high particle number or a high number of catalyst active sites per unit volume of the reactor (entry 3). One direct result is the large increase in local active sites/substrate ratio when the liquid is forced through the membrane pores (entry 5). The apparent reaction rate constant $k_{app}$ (entry 8) is the product of the specific catalyst surface $a$ (entry 11) and the intrinsic reaction rate on the catalyst surface $k$ (entry 12). The large catalyst number per unit volume value (entry 3) leads to a high specific surface (entry 11), which is mainly responsible for the reaction rate increase in the membrane. The difference on the intrinsic $k$ (entry 12) between the two systems depends on the particle size and distribution (entry 1), or more specifically, on the number of atoms on the PdNP surface. The ratio of number of atoms on the PdNPs surface (catalytic membrane/batch reactor) is estimated to be 1.4, and the ratio of number of vertex and edge atoms is calculated to be 2.9 (see the Supporting Information), which is close to the ratio of intrinsic reaction

rate constant $k$ (entry 12). The influence of $k$ on apparent kinetics (a factor of 1–3) should be much less remarkable than that exerted by the specific surface area $a$.

The conventional understanding of a forced flow-through membrane reactor is based on intensified contact between the catalyst and reactants being responsible for the reaction rate increase as local mass-transfer resistance can be effectively eliminated.[9,10] In consequence, improvements on mass transfer should not have obvious contributions to the apparent reaction rate when reactions were not diffusion-limited. However, for the Suzuki-Miyaura cross-coupling between 1-iodo-4-nitrobenzene and phenylboronic acid (kinetic-limited in the batch reactor), the kinetics was largely enhanced nonetheless in the catalytic membrane. A simple calculation can help to understand how the apparent reaction rate was accelerated in the catalytic membrane. The volume of the membrane used in the experiments was 0.14 cm$^3$. Hence taking into account the porosity, the liquid volume retained in the membrane was around 0.1 cm$^3$. For a concentration of 0.016 mol L$^{-1}$, the limiting reactant amount inside the membrane volume was $1.6 \times 10^{-6}$ mol. When the reaction solution was filtered through the membrane (where the catalyst got into contact with the reagents), the Pd/substrate molar ratio in the local environment of the membrane is ( = 4.7) 470 times higher than that in the batch reactor ( = 0.01). The real Pd/substrate molar ratio in the membrane can be even higher due to the heterogeneous catalyst distribution inside the membrane (there exist reactive zones inside the membrane where the catalyst is highly concentrated). To be more precise in describing the relative amount of reactant and catalyst, the ratio of catalyst surface to substrate amount should be compared (to reflect number of active sites) instead of Pd/substrate molar ratio (Table 1, entry 5).

It is also noteworthy that despite the high Pd/substrate ratio, the total palladium amount in the membrane is fairly low. The catalyst surface area ratio (catalytic membrane reactor/batch

reactor) is only around 2 (entry 4). It is important to note that the reaction time for full conversion in entry 6 refers to the contact time of reagents with the membrane.[3] The total filtration time (treating time) of the catalytic membrane reactor for the same amount of substrate as that in the batch reactor is around 30 min.[3] Hence the treating time of the catalytic membrane reactor is 12 times shorter than for the batch reactor. Besides, the catalytic membrane also exhibits the advantage of operating in a continuous manner. With the comparative factor of total catalyst surface area (entry 4) between the two systems much smaller than that of total treating time and reaction time (entry 6), it is clearly proved that the PdNPs size plays only a minor role in the high efficiency of the catalytic membrane reactor, which is in coherence with the small difference of the intrinsic reaction rate constant between the two systems (entry 12).

The high local Pd/substrate ratio can only be beneficial in forced flow-through configuration: every single volume of reaction solution is forced into the local high catalyst concentration environment. When the same membrane is submerged in a batch reactor, the catalytic performance will be no more outstanding.[27]

In brief, the Suzuki-Miyaura cross-coupling between 1-iodo-4-nitrobenzene and phenylboronic acid is not mass-transfer limited under batch conditions. The substantial reaction rate increase by the catalytic membrane reactor in forced flow-through configuration can be certainly attributed to the concentrating effect of the membrane (i.e., packing a large number of particles into a tiny volume). This is in agreement with the observation of Seto and coworkers,[5] who attributed the small rate constant of their Pd-loaded continuous-flow membrane reactor to the low concentration of Pd catalyst in the membrane reactor. They suggested that densification of the Pd catalyst in the membrane could lead to catalytic improvements. The convective flow in our case serves to eliminate the concentration gradient in the boundary layer at the membrane feed side surface and inside the membrane, bringing reactants from the bulk solution into the reactive membrane.

## Conclusions

The polymeric catalytic membrane reactor that we prepared was similar to, and thus can be considered as, a micro-reactor for its small characteristic dimensions (ca. $0.2 \mu m$). Theoretical calculations showed that a plug-flow behavior was always expected in the catalytic membrane pores. Therefore, there will be virtually no preferential flow pathways. The membrane reactor was also adapted for moderately exothermic reactions, achieving isothermal conditions.

It is indispensable to adopt the flow-through configuration when using the catalytic membrane reactor to attain a high catalytic activity. The convective flow brings the reagents into the catalyst highly concentrated membrane local environment where the reaction takes place. It also helps to eliminate the mass-transfer limit (in the boundary layer at the feed side as well as inside the membrane).

When the catalytic membrane reactor was employed, the Suzuki-Miyaura cross-coupling using 1-iodo-4-nitrobenzene as substrate was complete within 10 s without formation of any by-product. This reaction was in the reaction-limited regime in the batch reactor. Mathematical modeling of the catalytic membrane showed that there is a concentration boundary layer on the feed side of the membrane and that the reactant concentration gradient inside this boundary layer and

along the membrane thickness can be eliminated at high flux (by convection). These features explain the productivity increase with the flux increase. The much higher efficiency of the catalytic membrane (compared to the PdNPs dispersed in an IL under batch conditions) is principally attributed to the high local catalyst concentration inside the small membrane reactor volume since the intrinsic reaction rate constants of the membrane reactor and the batch reactor are of the same order of magnitude. PdNPs size (in the range of 1–6 nm) seems to exert a negligible effect on the reactivity.

## Notation

$a$ = catalyst specific surface area, $m^2 m^{-3}$
$C$ = limiting reactant concentration in the membrane, $mol\ m^{-3}$
$C_b$ = limiting reactant concentration in the bulk solution, $mol\ m^{-3}$
$C_{BL}$ = limiting reactant concentration in the boundary layer on the feed side of the membrane, $mol\ m^{-3}$
$C_e$ = limiting reactant concentration on the feed side surface of the membrane, $mol\ m^{-3}$
$C_f$ = limiting reactant concentration in the permeate, $mol\ m^{-3}$
$c$ = dimensionless concentration
$D$ = diffusion coefficient, $m^2 s^{-1}$
$d$ = pore diameter, m
$d_p$ = diameter of nanoparticles, m
$e$ = interparticle distance, m
$J$ = molar flux density, $mol\ m^{-2} s^{-1}$
$j$ = filtration flux density, $L\ h^{-1} m^{-2}$
$k$ = intrinsic reaction rate in either the batch reactor ($k_{batch}$) or the membrane ($k_{mem}$), $m\ s^{-1}$
$k_B$ = Boltzmann constant ($1.38 \times 10^{-23}\ J \cdot K^{-1}$), $J\ K^{-1}$
$k_{app}$ = apparent reaction rate, $s^{-1}$
$k_d$ = mass-transfer coefficient in either the batch reactor ($k_d^b$) or the membrane ($k_d^m$), $m\ s^{-1}$
$L$ = membrane thickness, m
$Pe_M$ = Péclet number inside the membrane
$Pe_{BL}$ = Péclet number in the boundary layer
$r$ = solute molecule radius, m
$S$ = total catalyst surface area, $m^2$
$Sc$ = Schmidt number
$Sh$ = Sherwood number
$T$ = temperature, K
$v_m$ = convective velocity in the membrane, $m\ s^{-1}$
$v$ = convective velocity in the bulk solution, $m\ s^{-1}$
$X$ = conversion
$Z$ = dimensionless coordinate
$z$ = space coordinate, m
$\varnothing$ = Thiele modulus
$\varepsilon$ = membrane porosity
$\rho$ = liquid density, $kg\ m^{-3}$
$\delta$ = momentum boundary layer thickness on the feed side of the membrane, m
$\delta_C$ = concentration boundary layer thickness on the feed side of the membrane, m
$\omega$ = agitation velocity, $rad\ s^{-1}$
$\mu$ = dynamic viscosity, $kg\ m^{-1} s^{-1}$
$\tau_{mix}$ = characteristic mixing time, s

## Literature Cited

1. Ozdemir SS, Buonomenna MG, Drioli E. Catalytic polymeric membranes: preparation and application. *Appl Catal A Gen*. 2006;307: 167–183.
2. Song IK, Lee WY. Heteropolyacid (HPA)-polymer composite films as heterogeneous catalysts and catalytic membranes. *Appl Catal A Gen*. 2003;256:77–98.

3. Gu Y, Favier I, Pradel C, Gin DL, Lahitte J-F, Noble RD, Gómez M, Remigy J-C. High catalytic efficiency of palladium nanoparticles immobilized in a polymer membrane containing poly(ionic liquid) in Suzuki–Miyaura cross-coupling reaction. *J Membr Sci*. 2015;492: 331–339.

4. Faria VW, Oliveira DGM, Kurz MHS, Goncalves FF, Scheeren CW, Rosa GR. Palladium nanoparticles supported in a polymeric membrane: an efficient phosphine-free "green" catalyst for Suzuki-Miyaura reactions in water. *RSC Adv*. 2014;4:13446–13452.

5. Seto H, Yoneda T, Morii T, Hoshino Y, Miura Y, Murakami T. Membrane reactor immobilized with palladium-loaded polymer nanogel for continuous-flow Suzuki coupling reaction. *AIChE J*. 2015;61:582–589.

6. Carlin RT, Fuller J. Ionic liquid-polymer gel catalytic membrane. *Chem Commun*. 1997;(15):1345–1346.

7. Domenech B, Munoz M, Muraviev D, Macanas J. Polymer-stabilized palladium nanoparticles for catalytic membranes: ad hoc polymer fabrication. *Nanoscale Res Lett*. 2011;6:406.

8. Emin C, Remigy J-C, Lahitte J-F. Influence of UV grafting conditions and gel formation on the loading and stabilization of palladium nanoparticles in photografted polyethersulfone membrane for catalytic reactions. *J Membr Sci*. 2014;455:55–63.

9. Tan X, Li K. *Inorganic Membrane Reactors: Fundamentals and Applications*. Chichester: Wiley, 2015.

10. Zaspalis VT, Van Praag W, Keizer K, Van Ommen JG, Ross JRH, Burggraaf AJ. Reactions of methanol over catalytically active alumina membranes. *Appl Catal*. 1991;74:205–222.

11. Nagy E. Diffusive plus convective mass transport through catalytic membrane layer with dispersed nanometer-sized catalyst. *Int J Compos Mater*. 2012;2:79–91.

12. Deraedt C, Astruc D. "Homeopathic" palladium nanoparticle catalysis of cross carbon–carbon coupling reactions. *Acc Chem Res*. 2014; 47:494–503.

13. Aris R. On the dispersion of a solute in a fluid flowing through a tube. *Proc R Soc Lond Ser A Math Phys Eng Sci*. 1956;235:67–77.

14. Nagy KD, Shen B, Jamison TF, Jensen KF. Mixing and dispersion in small-scale flow systems. *Org Process Res Dev*. 2012;16: 976–981.

15. Taylor G. Dispersion of soluble matter in solvent flowing slowly through a tube. *Proc R Soc Lond Ser A Math Phys Eng Sci*. 1953; 219:186–203.

16. Westermann T, Kretzschmar E, Pitsch F, Melin T. Heat transfer and temperature profiles in flow-through catalytic membrane reactors. *Chem Eng J*. 2009;155:371–379.

17. Dortmund Data Bank Software & Separation Technology GmbH. *Data Base for Dynamic Viscosity of Ethanol, Thermal-Fluids Central Encyclopedia*, 2015. https://www.thermalfluidscentral.org/encyclopedia/index.php/Thermophysical_Properties:_Ethanol

18. Langmuir I. The velocity of reactions in gases moving through heated vessels and the effect of convection and diffusion. *J Am Chem Soc*. 1908;30:1742–1754.

19. Landau LD, Lifshitz EM. *Fluid Mechanics*. Oxford: Pergamon Press, 1987.

20. Becht NO, Malik DJ, Tarleton ES. Evaluation and comparison of protein ultrafiltration test results: dead-end stirred cell compared with a cross-flow system. *Sep Purif Technol*. 2008;62:228–239.

21. Friedlander SK. A note on transport to spheres in stokes flow. *AIChE J*. 1961;7:347–348.

22. Nagy E, Blickle T, Ujhidy A. Spherical effect on mass transfer between fine solid particle and liquid accompanied by chemical reaction. *Chem Eng Sci*. 1989;44:198–201.

23. Atilhan M, Jacquemin J, Rooney D, Khraisheh M, Aparicio S. Viscous behavior of imidazolium-based ionic liquids. *Ind Eng Chem Res*. 2013;52:16774–16785.

24. Jacquemin J, Husson P, Padua AAH, Majer V. Density and viscosity of several pure and water-saturated ionic liquids. *Green Chem*. 2006; 8:172–180.

25. Leybros J, Frémeaux P. Extraction solide-liquide, aspects théoriques. *Technique de l'Ingénieur*. J2780.

26. Cai L-H, Panyukov S, Rubinstein M. Mobility of nonsticky nanoparticles in polymer liquids. *Macromolecules*. 2011;44:7853–7863.

27. Gu Y, Remigy JC, Favier I, Gómez M, Noble RD, Lahitte JF. Membrane reactor based on hybrid nanomaterials for process intensification of catalytic hydrogenation reaction: an example of reduction of the environmental footprint of chemical synthesis from a batch to a continuous flow chemistry process. *Chem Eng Trans*. 2016;47: 367–372.